Supplementary Information
for:

The ABC-F protein EttA gates ribosome entry into the translation elongation cycle

Grégory Boël [1,2], Paul C. Smith [1†], Wei Ning [3], Michael T. Englander [3,4†], Bo Chen [1], Yaser Hashem [5], Anthony J. Testa [1], Jeffrey J. Fischer [6†], Hans-Joachim Wieden [6], Joachim Frank [1,5], Ruben L. Gonzalez Jr. [3§], and John F. Hunt [1,2§]

[1] Department of Biological Sciences, Columbia University, New York, NY, USA;

[2] Northeast Structural Genomics Consortium, Columbia University, New York, NY, USA;

[3] Department of Chemistry, Columbia University, New York, NY, USA;

[4] Integrated Program in Cellular, Molecular and Biomedical Studies, Columbia University, Medical Center, New York, NY, USA;

[5] Department of Biochemistry and Howard Hughes Medical Institute, Columbia University Medical Center, New York, NY, USA;

and

[6] Department of Chemistry and Biochemistry, University of Lethbridge, Lethbridge, AB, Canada.

[†] Present addresses: P.C.S: Department of Molecular Biology, Memorial Sloan-Kettering Cancer Center, New York, NY, USA; M.T.E: Department Biochemistry and Biophysics, University of Pennsylvania, Philadelphia, PA, USA; J.J.F: Department of Biological Sciences, University of Calgary, Calgary, AB, Canada.

[§] To whom correspondence may be addressed:
e-mail jfhunt@biology.columbia.edu, voice (212)-854-5443, FAX (212)-865-8246 (JFH);
e-mail rlg2118@columbia.edu, voice (212)-854-1096, FAX (212)-854-1096 (RLG).

Keywords: Protein synthesis, translational regulation, ABC-F protein family, YjjK, ATP/ADP ratio, stationary phase fitness, X-ray crystallography.

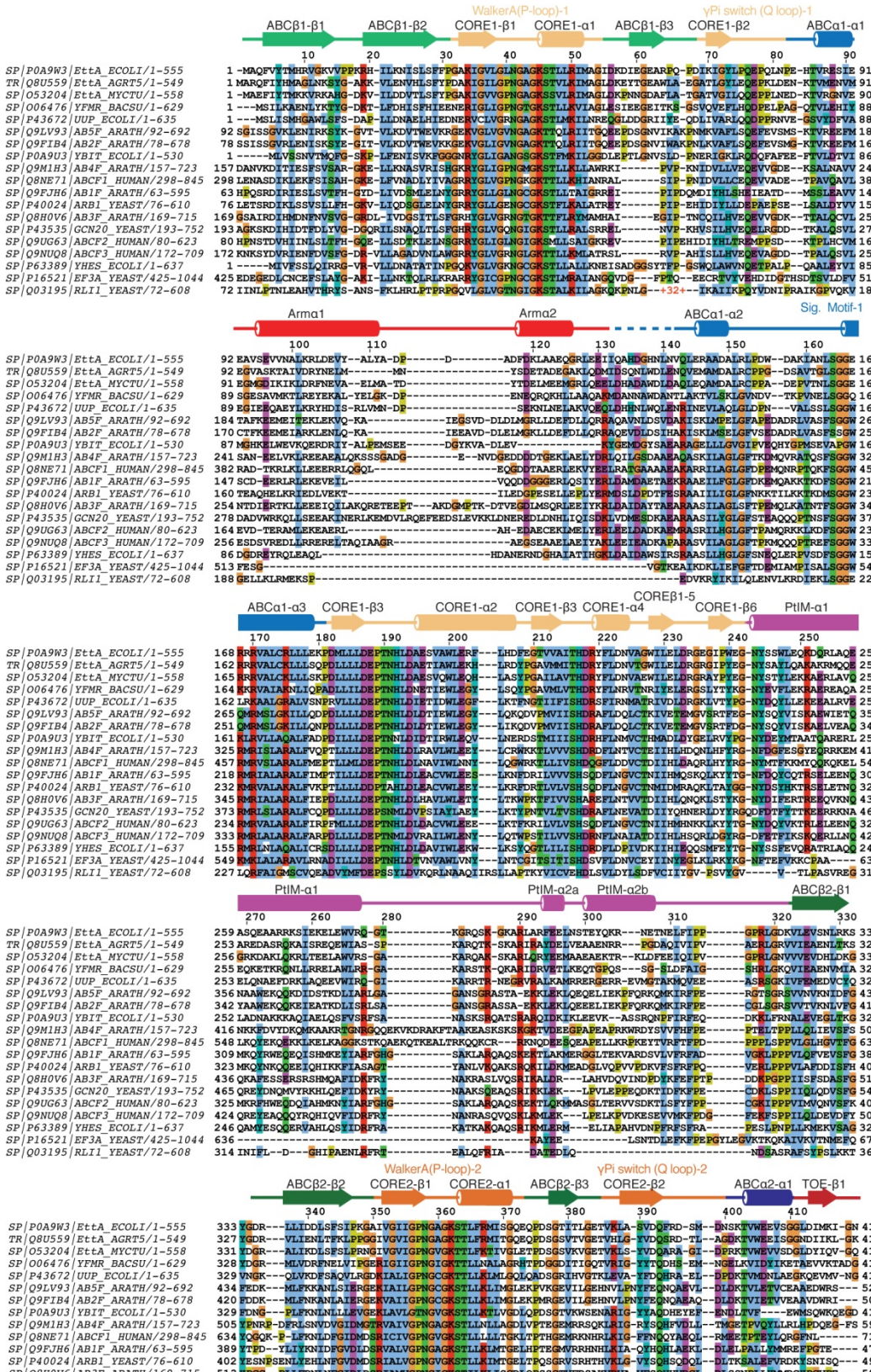

Nature Structural and Molecular Biology: doi:10.1038/nsmb.2740

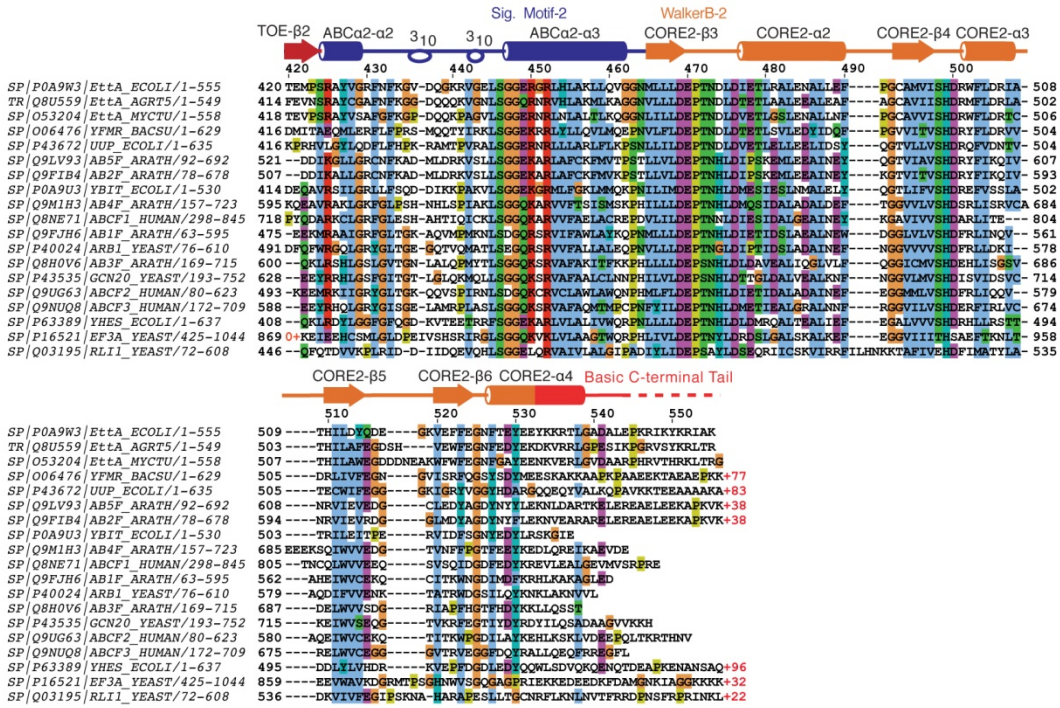

Supplementary Figure 1: ***Structure-based ABC-F sequence alignment.*** The secondary structural elements observed in the crystal structure of *E. coli* EttA are shown above the sequence alignment, with α-helices represented by cylinders, β-strands by arrows, and 3_{10} helices by circles. Secondary structure elements are colored as in **Fig. 2a** in the main text. The disordered protein segments are represented by dotted lines. The alignment shows EttA orthologues from *E. coli* (ECOLI), *A. tumefaciens* (AGRT5), *M. tuberculosis* (MYCTU) and *B. subtillis* (BACSU), as well as the three additional ABC-F proteins from *E. coli* (YheS, Uup, and YbiT), the three ABC-F in humans (ABCF1, 2 and 3), the two ABC-F (ARB1 and GCN20) and two other non-ABC-F soluble ABC (EF3A and ABCE1/RNaseLI (RLI1)) from *S. cerevisiae* (yeast). The alignment was initially generated using CLUSTAL-Ω [1] via the Uniprot website (http://www.uniprot.org/) and then manually edited using Jalview [2] to correctly align the Q loop motifs in all sequences and to accurately represent the structural alignment of EttA to the other ABC domains of known structure. The alignment is colored according to the default CLUSTAL coloring code. Large insertions compared to EttA were truncated, and the number of residues removed at each such site is indicated in red and flanked by "+" signs in the text of the alignment.

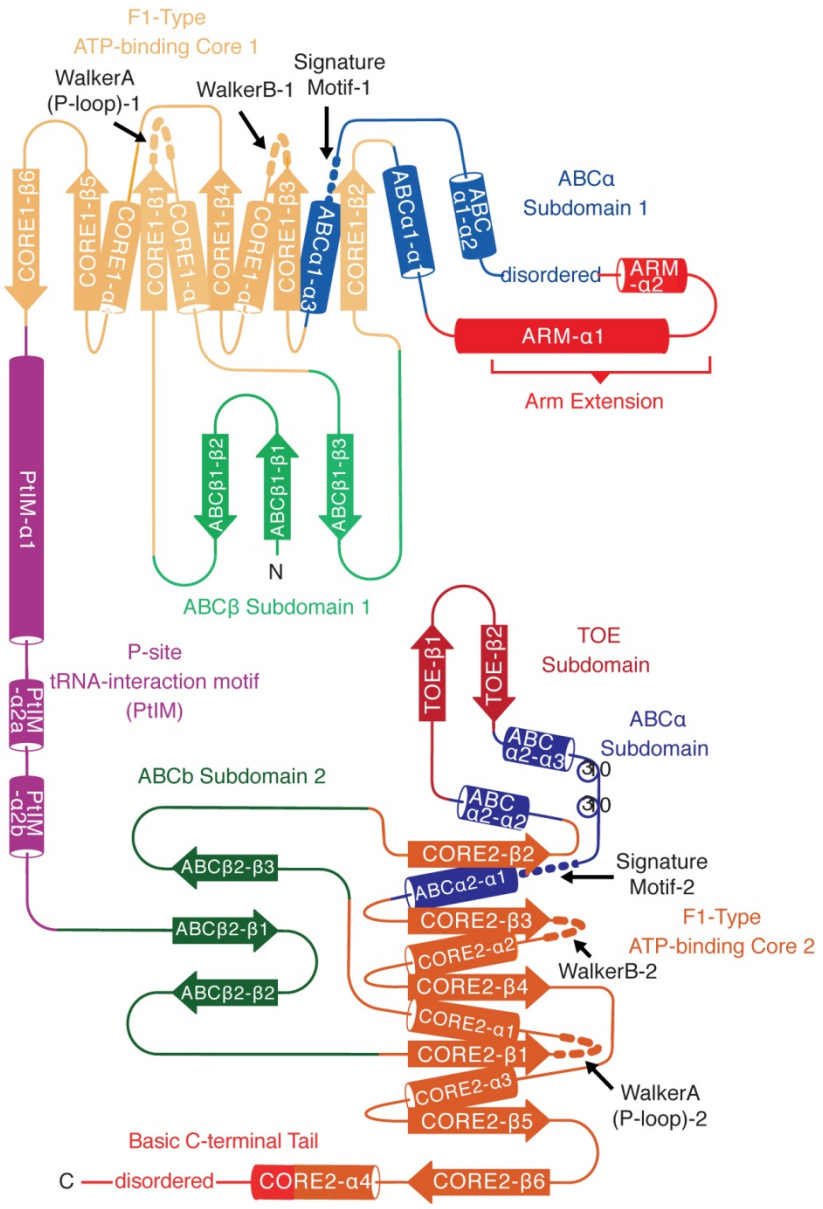

Supplementary Figure 2: ***Topology diagram of EttA.*** Secondary structure elements are colored as in **Fig. 2a**, with β-strands represented by arrows, α-helices represented by cylinders, and turns of 3_{10} helix represented by circles. The locations of the Walker A, Walker B, and ABC Signature (LSGGQ/E) motifs involved in ATP binding are indicated by thick dashed lines. The locations of disordered segments in the crystal structure are also indicated.

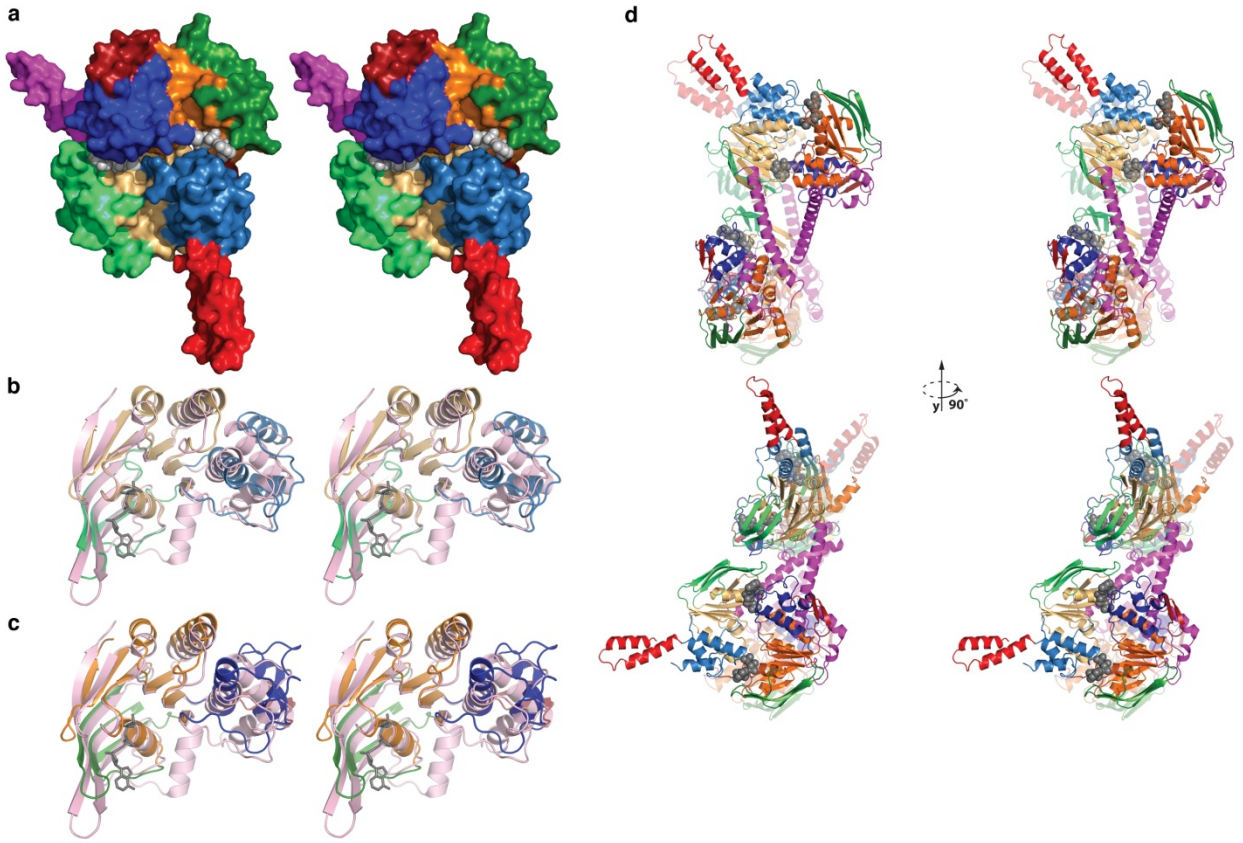

Supplementary Figure 3: ***Variations in ABCα subdomain alignment in the crystal structure of the E. coli EttA dimer*****.** **(a**) Stereopair showing the molecular surface of a model for the ATP-bound conformation of ABC1 and ABC2 in EttA, which was produced by applying a rigid-body rotation to one protomer in the crystallographically observed EttA dimer (as described in the legend for **Fig. 2b** in the main text). The structure is colored according to subdomain in an equivalent manner to Fig. 2 in the main text and Supplemental Fig. 1-2 above. The ATP molecules shown in gray space-filling representation are from the Na-ATP-bound MJ0796 dimer, which was used to model the ATP-bound EttA conformation as described above. This surface representation demonstrates that the ATP-binding site on the right, which is at the interface of the ABCα subdomain in ABC1 and the ABCβ and F1-like core subdomains in ABC2, is more open that the ATP-binding site on the left, which is formed by the ABCα subdomain in ABC2 and the ABCβ and F1-like core subdomains in ABC1. This asymmetry is attributable primarily to the different alignments of the ABCα subdomain relative to the F1-like core subdomain in ABC1 *vs.* ABC2, as shown in panels **b-c** below in this figure. **(b,c)** Stereo ribbon diagrams showing ABC1 (panel **b**) or ABC2 (panel **c**) from EttA superimposed on a protomer from the Na-ATP-bound dimer of the E171Q mutant of MJ0796 (PDB id 1L2T), based on least-squares alignment of the ABCβ and F1-like core subdomains. The EttA subdomains are colored like panel **a** above, while MJ076 is colored pink. These images show that, in the nucleotide-free crystal structure of EttA, the ABCα and F1-like core subdomains within each ABC domain are rotated relative to one another by 18-20˚ compared to their alignment in the canonical ATP-binding conformation. Similar reorientations of these subdomains have been

observed in other ABC domain structures that do not have the γ-phosphate group of ATP bound in the active site [3,4]. Formation of the catalytically active complex upon ATP binding to EttA presumably involves relative rotation of the ABCα and F1-like core subdomains within both the ABC1 and ABC2 domains as well as a mutual rotation of these domains (as modeled in **Fig. 2c**) to bring them into the canonical ATP-sandwich conformation observed in the ATP-bound structures of other ABC proteins [5-7]. **(d)** Observed *apo* structure and modeled ATP-bound conformation of the *E. coli* EttA dimer. Stereo ribbon diagrams of a model for the ATP-bound (solid colors) conformation superimposed on the crystallographically observed nucleotide-free conformation (translucent colors), based on least-squares alignment of the B protomers. The crystallographically observed *apo* structure (**Table 1**) was used to model the ATP-bound conformation by aligning the ABCβ and F1-like core subdomains in ABC1 and ABC2 in different EttA protomers to the protomers in the Na-ATP-bound dimer of the E171Q mutant of MJ0796 (PDB id 1L2T). ATP molecules from the MJ0796 dimer are represented in gray space-filling representation. The structures are colored as in **Fig. 2** in the main text and oriented such that the interface of one of the two ABC1-ABC2 interfaces in the EttA dimer is visible in each of the two views, which are related by a 90˚ rotation around a vertical axis.

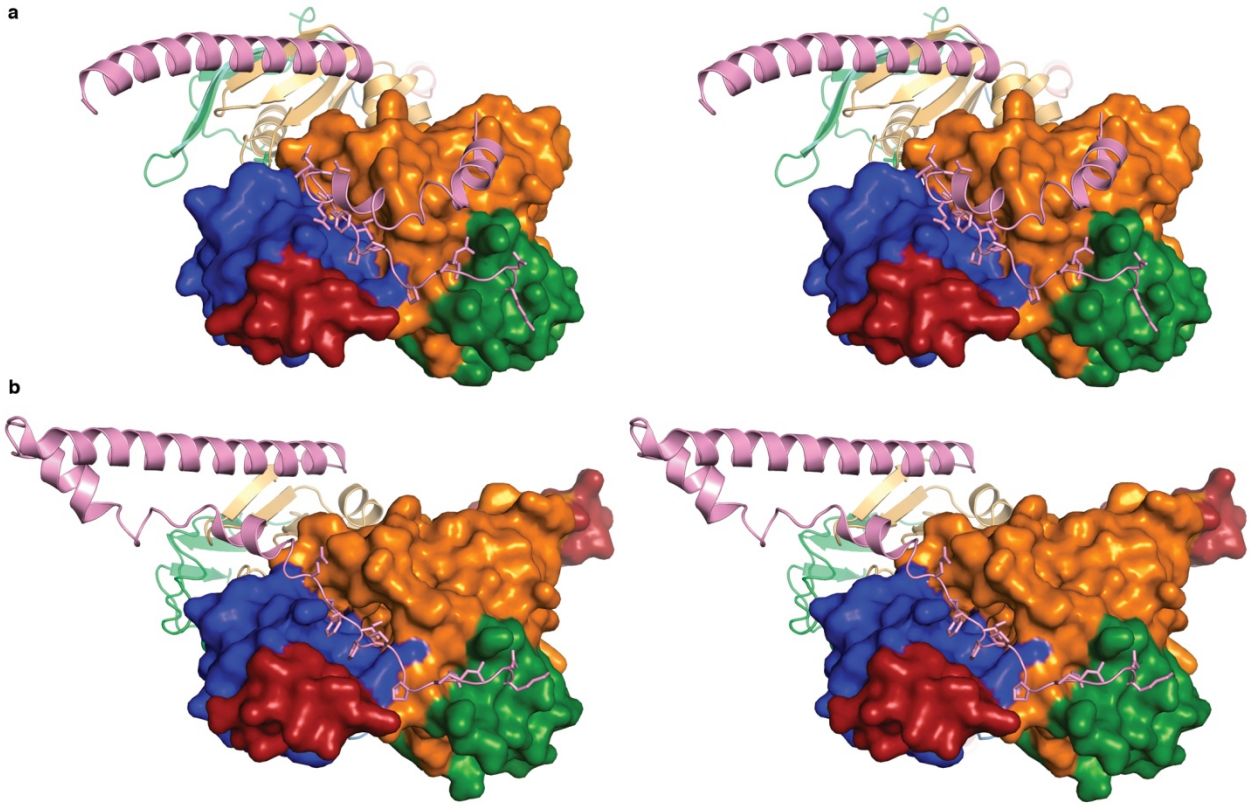

Supplementary Figure 4: ***Conformational change in the PtIM in the EttA monomer vs. dimer and the packing interactions of the C-terminus of PtIM.*** These stereopairs show the molecular surface of ABC2 and a ribbon representation of ABC1 and the PtIM (*i.e.*, the interdomain linker between ABC1 and ABC2), colored like **Fig. 2** in the main text. **(a)** Crystallographically observed *apo* conformation of one ABC1-ABC2 domain pair in the EttA dimer (**Supplementary Fig. 3** and **Table 1**). This image was generated as described for **Fig. 2b** in the main text, *i.e.*, by deletion of all the residues prior to the Lys 286 in the protomer A and deletion of all the residues after the Gln 278 in the protomer B. **(b)** ATP-bound conformation of the EttA monomer modeled from the cryo-EM structure of EttA-EQ_2 bound to 70S ribosomes, as presented in the accompanying paper [8]. Two α-helices from the C-terminal half of the PtIM that pack onto the surface of ABC2 in the dimer structure (panel **a**) must undergo a conformational change to enable ABC1 and ABC2 in a single protomer to interact with one another in proper geometry in the EttA monomer (panel **b**). The C-terminal segment of the PtIM (*i.e.*, the segment after that undergoing the conformational change but before the start of ABC2) packs into a crevice at the interface between the ABCβ subdomain and the F1-like core subdomain in ABC2. The crystallographically observed conformation of these C-terminal residues in the PtIM could modulate the relative rotation of ABCα and F1-like core subdomains required to adopt the catalytically active nucleotide-sandwich conformation (described in **Supplemental Fig. S3b-c**). The cryo-EM structure of ribosome-bound EttA[8] shows that the latter two α-helices in the PtIM refold compared to their crystallographically observed conformation to form a long α-helical hairpin in conjunction with the first α-helix in the PtIM (panel **a** *vs.* **b**), which remains intact. This conformational change in the PtIM is likely to be coupled to dissociation of the EttA dimer that is observed in its crystal structure.

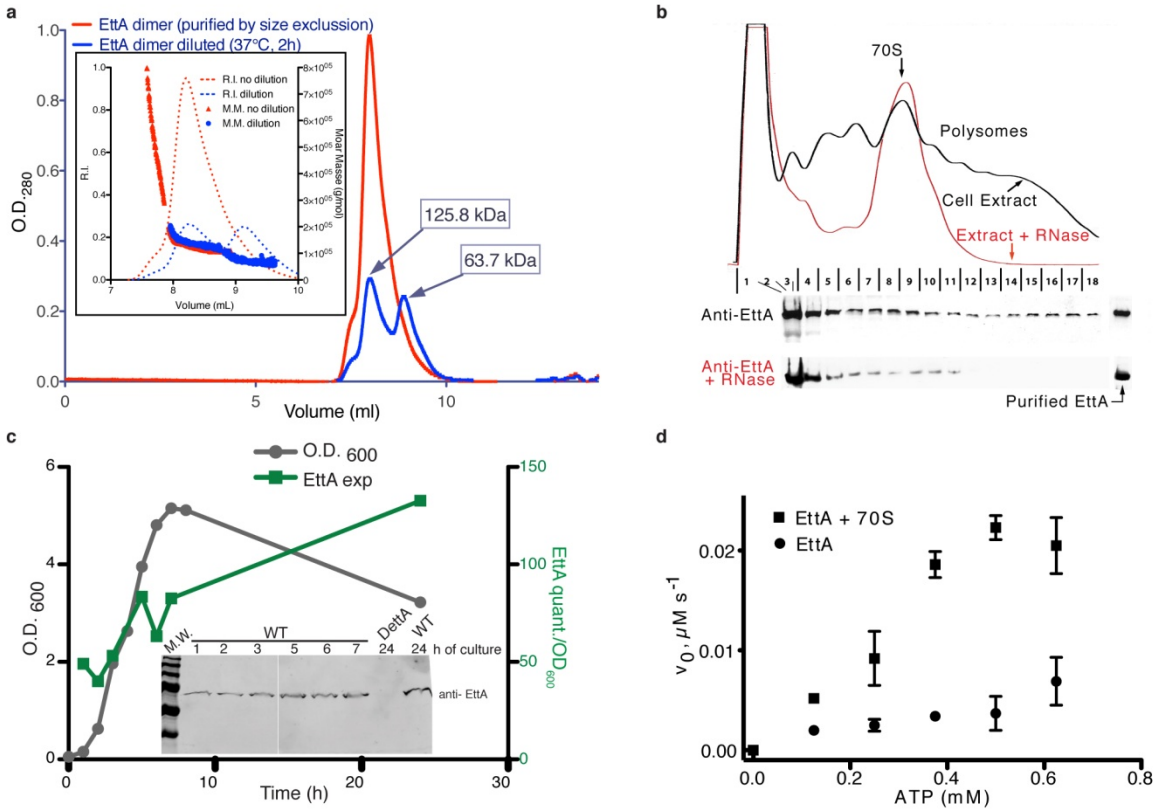

Supplementary Figure 5: ***Further characterization of EttA in vitro and in vivo.*** **(a)** Gel filtration analysis of purified *E. coli* EttA shows a slow but reversible monomer-dimer equilibrium**.** Analytical gel-filtration chromatography on a system equipped with in-line UV, refractive index (RI), and static light-scattering detectors (SLS) detectors was used to analyze two samples of WT EttA at different concentrations. A protein fraction from the leading edge of the peak from a preparative gel-filtration column, representing the final step in the purification of EttA, was either injected directly onto an analytical gel-filtration column (red trace) or diluted 1:1 in the elution buffer and heated for 2 hours at 37 °C prior to injection onto the same analytical gel-filtration column (blue trace). The insert shows equivalently color-coded plots of the RI (left axis and dotted lines) and calculated molar mass (right axis and solid lines) *vs.* volume for these two chromatograms. The same volume of protein solution (100 µl) was injected for both of the analytical gel filtration runs displayed here. Debye analyses of the SLS/RI data indicate that the single peak in the black trace and the earlier peak in the gray trace have a mass-averaged molecular weight of ~126 kDa, consistent with the presence of an EttA dimerA (based on the 62.4 kDa predicted molecular weight of the protomer). Debye analysis of the second peak in the gray trace indicates a mass-averaged molecular weights of ~64 kDa, consistent with the presence of an EttA monomer. Concentration of this monomer peak and re-injection on an analytical gel-filtration column shows a mixture of monomer and dimer. Analytical gel filtration chromatography was conduced on a Shodex 804 column running at 4 ˚C with a 0.5 ml/min flow-rate in 150 mM NaCl, 5% glycerol, 20mM Tris-HCL, pH 7.2. SLS and RI detectors were from Wyatt Technology. **(b)** *E. coli* EttA protein co-fractionates with polysomes. An extract of mid-log phase cultures of *E. coli* was fractionated using sucrose density

gradient sedimentation either without (black trace and upper gel) or with (red trace and lower gel) RNaseA treatment. The optical density of the gradients at 254 nm is shown above immunoblots of the corresponding fractions developed using a polyclonal anti-EttA antiserum. RNaseA treatment cleaves the mRNA holding the polysomes together to yield single fully assembled ribosomes (containing both large and small subunits) that sediment at 70S. **(c)** Analysis of variations in EttA expression level during the *E. coli* life cycle. WT or Δ*ettA* MG1655 cells were inoculated into fresh LB medium, and the cultures were monitored during 24 hours of growth at 37 ˚C. The graph is showing the OD_{600} of the MG1655 culture in gray (right axis) and the intensity of the signal on the immunoblot in green (left axis). The near-IR fluorescence recorded from the immunoblot was quantified using ImageJ[9] software. Insert, Western blot analysis of total cells extracts using a polyclonal anti-EttA antibody, after growth for the number of hours indicated at the top of the blot. **(d)** Stimulation of EttA ATPase activity by 70S ribosome. Initial velocity of ATP hydrolysis (vertical axis) was measured as a function of ATP concentration (horizontal axis) for WT EttA alone or in the presence of 70S *E. coli* ribosomes. Assays were performed in polymix buffer (5 mM Tris-acetate (pH 7.5), 95 mM KCl, 5 mM NH_4Cl, 5 mM $Mg(OAc)_2$, 0.5 mM $CaCl_2$, 2 mM 2-mercaptoethanol, 5 mM putrescine, and 1 mM spermidine).

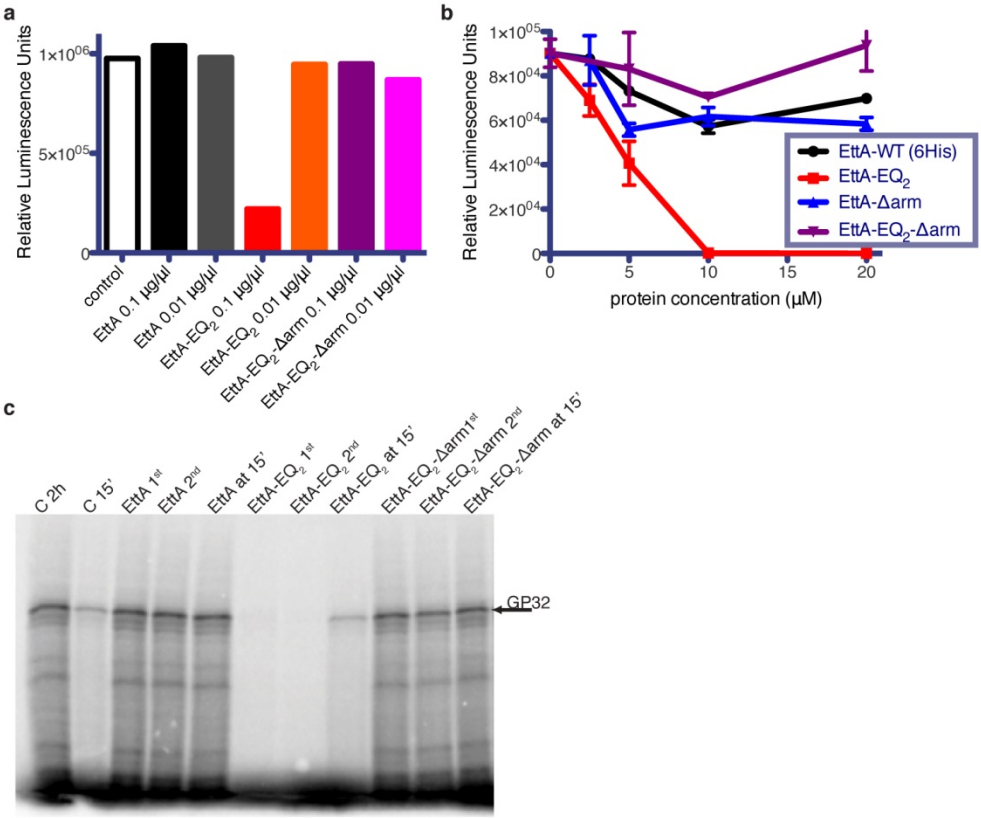

Supplementary Figure 6: ***EttA-EQ$_2$ inhibits protein translation in vitro in complete and minimum translation assays.*** **(a)** Luminescence assays were used to quantify the level of *in vitro* translation of luciferase from T7-*luc* mRNA using a complete *in vitro* translation system, specifically the *E. coli* S30 Extract System for Linear Templates (Promega). Briefly, reactions containing the indicated EttA variant (or an equivalent volume of buffer) were started by adding T7-*luc* mRNA and incubated at 37 ˚C for 2 hours prior to conducting luciferase activity assays using a luminometer. Background from a reaction without T7-*luc* mRNA was subtracted from the values reported here. See the Methods section for details. **(b)** Equivalent luminescence assay were used to quantify the level of *in vitro* translation of luciferase from the same mRNA template using a minimal *in vitro* translation system, specifically the PURExpress System (New England Biolabs). These reactions were conducted in triplicate in 96-well plates, which were incubated at 37 ˚C for 2 hours prior to conducting luminescence assays using a microplate reader. **(c)** Autoradiography was used to assay *in vitro* translation of the bacteriophage T4 pg32 protein using the PURExpress system (New England Biolabs). EttA variants were added to a final concentration of 5 µM, and reactions programmed with pT7gp32.1-224 mRNA were incubated at 37 ˚C for 2 hours prior to autoradiography of samples run a 12.5% (w/v) SDS-PAGE gel. Each EttA variant was added either before the mRNA (labeled "1st"), immediately after the mRNA (labeled "2nd"), or 15 min after addition of the mRNA (labeled "at 15'").

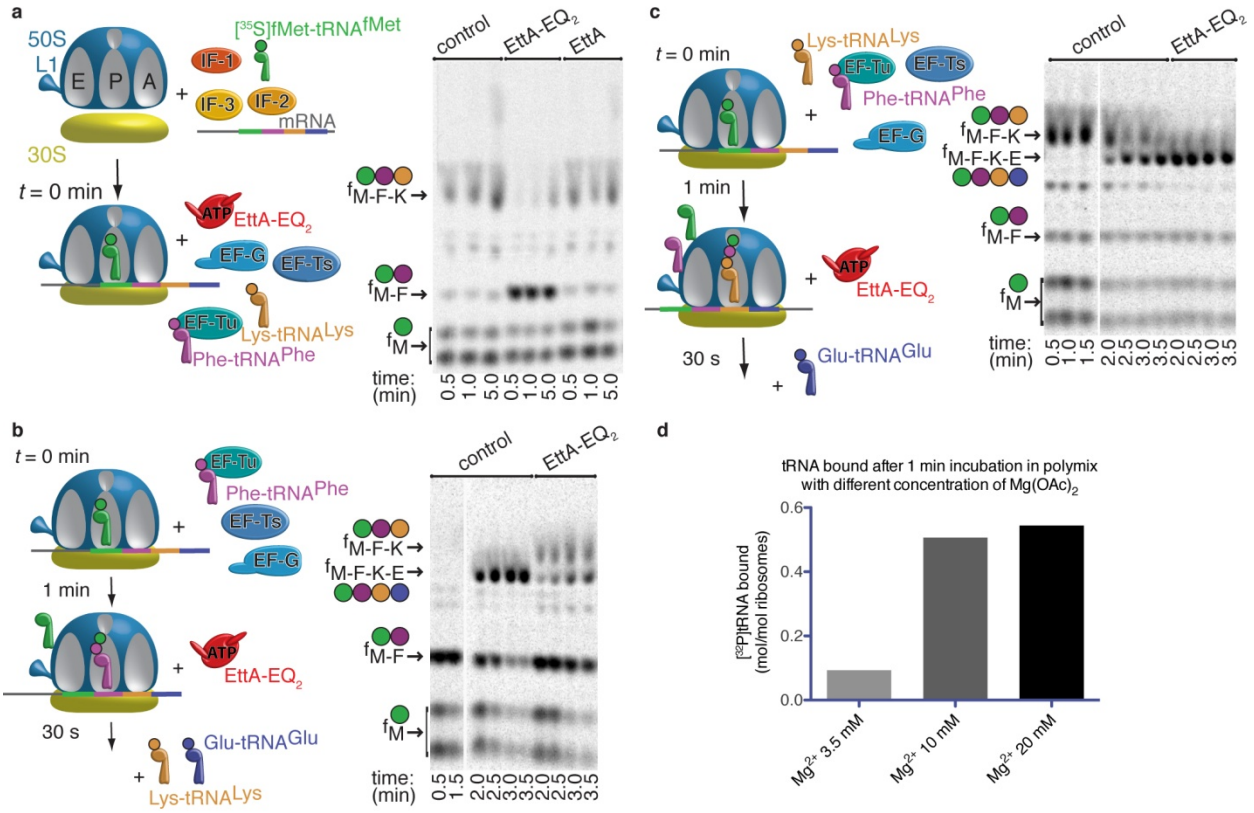

Supplementary Figure 7: ***Order-of-addition experiments demonstrate that EttA-EQ$_2$ acts after 70S IC formation to trap ribosomes following dipeptide formation and that it can stimulate peptide-bond formation on the ribosome.*** Minimum *in vitro* translation assays were conducted as in **Fig. 4** in the main text in the presence of 0.5 mM Mg-ATP but with variations in the timing of addition of some components, as illustrated in the schematic diagrams on the left in panels **a-c**. Ribosomally synthesized peptides, up to 4 amino acids in length, were separated and quantified by autoradiography of eTLC plates, as shown on the right in panels **a-c**. **(a)** Addition of EttA-EQ$_2$ before or after formation of the 70S IC produces an equivalent inhibition of translation following dipeptide formation. The tripeptide synthesis experiment shown here, in which EttA was added before 70S IC formation, gives equivalent results to the experiment shown in **Fig. 4a** in the main text, in which EttA was added after 70S IC formation. Translation reactions were started by adding the elongation factors and Phe-tRNA^{Phe} and Lys-tRNA^{Lys}. **(b)** Addition of EF-G prior to EttA-EQ$_2$ reduces the extent of inhibition of protein translation but does not lead to strong accumulation of tripeptide in a tetrapeptide synthesis assay. Translation reactions containing EF-G were set up to stop after dipeptide synthesis due to lack of a cognate tRNA for the third codon in the model mRNA. Inclusion of EF-G in these reactions should result in translocation of the dipeptide-bearing tRNA to the P site in a substantial fraction of ribosomes. Subsequent addition of EttA-EQ$_2$ inhibits dipeptide elongation in these assays much less effectively than in assays in which translocation of the dipeptide-bearing tRNA has been prevented by omission of EF-G prior to the addition of EttA (**Fig. 4b** in main), showing that it acts preferentially on the pretranslocation complex with deacylated tRNA^{fmet} in the A site of the

ribosome. Moreover, tetrapeptide is formed in higher yield than tripeptide in these assays in which EF-G is added to translation reactions before EttA-EQ_2, demonstrating that it inhibits elongation of dipeptides more strongly than that of tripeptides, again consistent with it acting preferentially on ribosomes bearing $tRNA^{fmet}$ in the P site. **(c)** Addition of EttA-EQ_2 after tripeptide synthesis on the ribosome complex modestly stimulates tetrapeptide synthesis rather than inhibiting it. Translation reactions were set up in presence of EF-G with cognate tRNAs for the first three but not the fourth codon in the mRNA, thereby stopping translation after tripeptide synthesis. EttA-EQ_2 was subsequently added prior to addition of the cognate tRNA for the fourth codon. The modest stimulation of tetrapeptide synthesis in this experiment provides evidence that interaction of the ATP-bound conformation of EttA with ribosomes promotes peptide-bond formation in the peptidyl-transferase center. The results of this experiment also support the conclusion that EttA-EQ_2 does not inhibit post-translocation ribosomal complexes because it specifically blocks the translocation step in the ribosomal elongation cycle. **(d)** Filter-binding assay showing that the ribosomal E site does not stably retain deacylated tRNAs at the Mg^{2+} concentration used in standard translation assays. The retention of 0.4 μM deacylated $[^{32}P]tRNA^{Phe}$ by 70S ribosomes was assayed in the presence of different concentrations of $Mg(OAc)_2$ (3.5, 10, and 20 mM). Assays were conducted using a 0.2 μM concentration of 70S ribosomes in 0.1 M NH_4Cl, 20 mM Tris-HCl, pH 7.4. At 3.5 mM Mg^{2+}, which is the concentration used in the minimum *in vitro* translation reactions, the deacylated tRNA is not retained on the E site of the ribosome, even through it is retained at the higher Mg^{2+} concentrations. This observation indicates that EttA-EQ_2 should have access to the E site in the post-translocation complex prepared in the experiment shown in panel **c**, consistent with the interpretation that binding of EttA-EQ_2 at this site stimulates peptide bond formation in the peptidyl-transferase center on the ribosome.

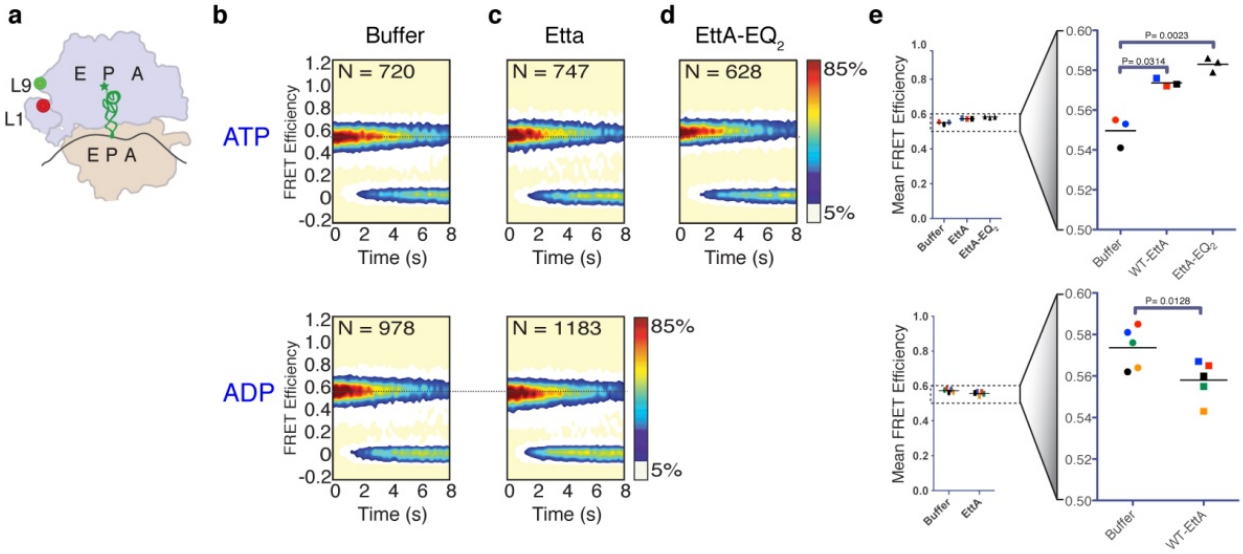

Supplementary Figure 8: ***Characterization of EttA interactions with the 70S IC using the smFRET$_{L1-L9}$ signal.*** (**a**) Cartoon diagram of the 70S IC used in these experiments. The 30S and 50S subunits of the ribosome are shown in tan and blue, respectively. The fMet-tRNA^{fMet} is represented by a green ribbon, while the mRNA is represented by a black curve. The Cy3 donor and Cy5 acceptor fluorophores are represented by green and red circles, respectively. (**b-d**) Data from smFRET$_{L1-L9}$ experiments recorded in the presence of either 2 mM Mg-ATP (top panels) or 2 mM Mg-ADP (bottom panels) and either in the absence of EttA (panel **b**), in the presence of 6 μM WT-EttA (panel **c**), or in the presence of 6 μM EttA-EQ$_2$ (panel **d**). These surface contour plots show the time evolution of the FRET efficiency (E_{FRET}) distribution in an ensemble of individually observed 70S ICs. The plots were generated by superimposing a large set of individual E_{FRET} *versus* time trajectories as previously described[10]; the variable *N* shown on each plot indicates the number of superimposed trajectories. The contours are color-coded as calibrated by the color bars shown on the right, with white and red representing the lowest and highest populated E_{FRET} levels, respectively. (**e**) Vertical column scatter plots showing the mean E_{FRET} values measured in a series of independent smFRET$_{L1-L9}$ experiments conducted in the presence of either Mg-ATP (top panel, three independent experiments) or Mg-ADP (bottom panel, five independent experiments). A plot encompassing the full E_{FRET} range (0.0–1.0) is shown on the left side of each panel, while an expanded view of the relevant E_{FRET} range (0.5–0.6) is shown on the right side of each panel. Independent experiments in the absence or presence of WT-EttA were recorded in a paired fashion (*i.e.*, with data collected from the same flowcell before and after adding WT-EttA). The mean E_{FRET} values from experiments conducted in the same flowcell are shown in the same color. Independent experiments in the absence or presence of EttA-EQ$_2$ were recorded in an unpaired fashion (*i.e.*, with data collected from different flowcells). The back horizontal lines on the graphs represent the mean E_{FRET} value for each experimental condition, while the p-values for the observed differences between the experimental conditions are shown at the top of each scatter plot. The p-values were calculated in version 5 of the program PRISM (Graphpad Inc.) using a paired t-test for WT-EttA and an unpaired t-test for EttA-EQ$_2$.

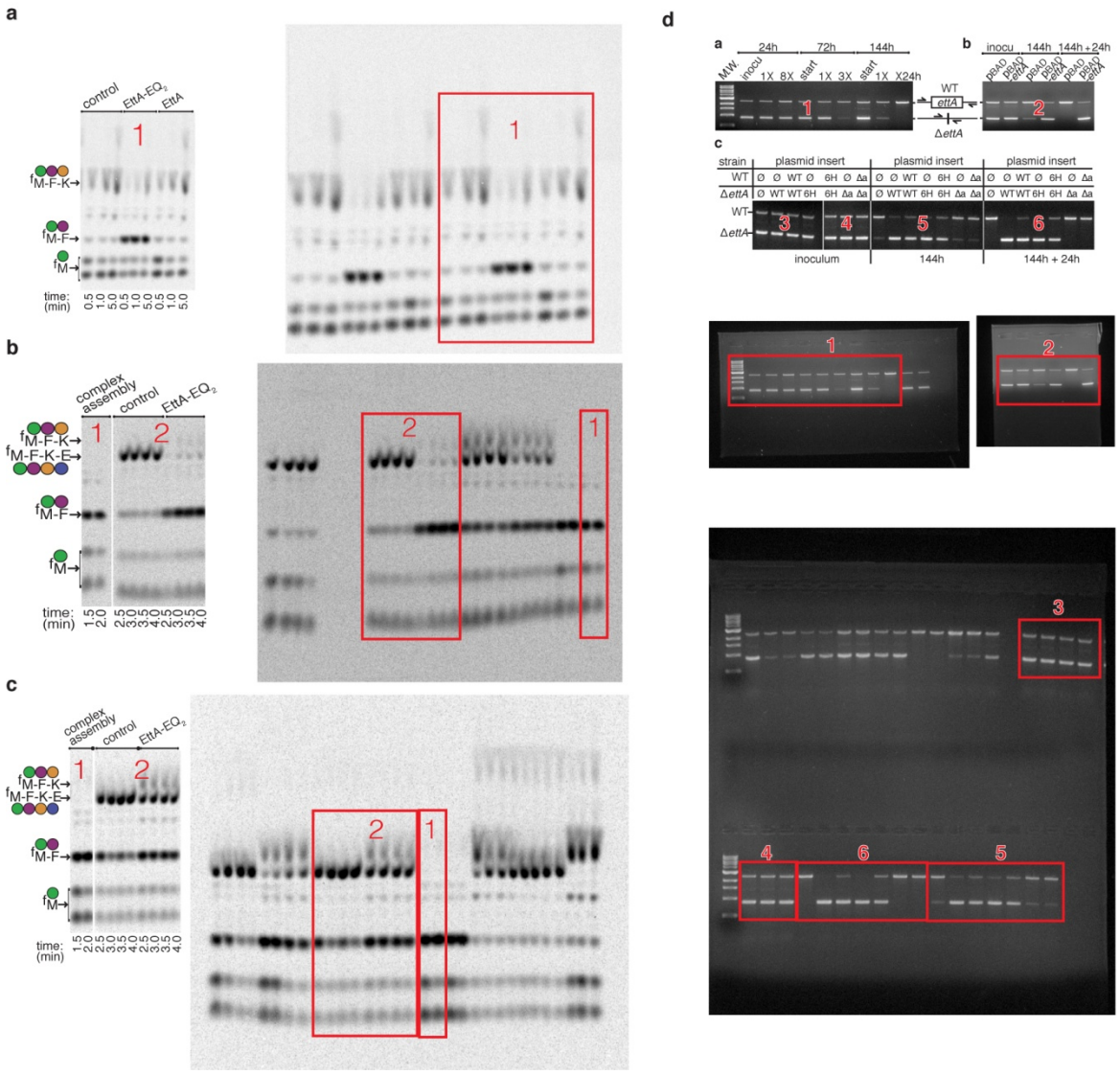

Supplementary Figure 9: ***Full view of the cropped eTLC plates and agarose gels presented in Figures 4 and 6 in the main text.*** (**a**) Miniature cropped eTLC data presented in **Figure 4a** (left) and the corresponding uncropped eTLC plate (left), with the red rectangle delimiting the area presented on the left**.** (**b**) Miniature cropped eTLC data presented in **Figure 4b** (left) and the corresponding uncropped eTLC plate (left), with the red rectangles delimiting the two areas (1 and 2) presented on the left**.** (**c**) Miniature cropped eTLC data presented in **Figure 4c** (left) and the corresponding uncropped eTLC plate (left), with the red rectangles delimiting the two areas (1 and 2) presented on the left**.** (**d**) Miniature cropped DNA agarose gels presented in **Figure 6** (top) and the corresponding uncropped agarose gels (center and bottom); the red rectangles delimit the 6 areas (1 to 6 in red) presented in the miniature of **Figure 6** (top)**.**

SUPPLEMENTARY TABLES

Supplementary Table 1A. ***Closest structural homologs to ABC1 of E. coli EttA as identified by DALI.*** [a]

		ABCβ+Core 1					ABCα 1				
Protein	PDB	Rank	Z-score	rmsd (Å)	% id	length	Rank	Z-score	rmsd (Å)	% id	length
EttA-ABC2		1	19.4	2.0	36	138	23	6.1	2.5	26	50
MalE	2R6G(B)	2	18.8	1.9	27	140	5	7.2	1.7	34	56
MJ0796	1L2T(B)	3	18.6	1.5	31	138	27	5.6	2.2	24	58
CFTR [b]	2PZE(B)	4	18.6	2.2	24	139	26	5.7	1.8	23	52
ArtP	2OLK(B)	5	18.3	2.1	28	141	21	6.4	1.9	29	56
LolD	2PCJ(A)	6	17.9	1.8	30	139	17	6.4	1.6	31	51
BtuD	4DBL(D)	9	17.7	1.8	29	135	1	8.1	1.8	27	55
RLI	1YQT(A)	12	17.4	1.9	28	138	12	7.0	1.5	39	49
EF3	2IX3(B)	24	15.9	2.2	31	134	19	6.5	1.6	22	50

[a] The ABCβ subdomain and F1-like core subdomain were submitted to the DALI server[11] for analysis together, but the ABCα subdomain was submitted separately because of its variable alignment in different structures was determined without the γ-phosphate of ATP bound in the ATPase active site (Supplementary Fig. 3a-c). The letter in parentheses in the PDB id is the chain identifier of the aligned subunit. The Rank represents the highest position of the aligned protein molecule when the list of structures with significantly structural similarity is sorted by decreasing Z-score (*i.e.*, ignoring structures giving lower Z-scores containing the same protein). The Z-score is a standard measure of statistical significance (given by the ratio of the difference between the structural similarity score and the mean score when scanning the database to the standard deviation in that score). The abbreviation rmsd stands for root-mean-square deviation. The % id represents the percent of identical amino acids in the aligned regions of the structures, while length is the number of residues included in these regions.

[b] This structure represents the first nucleotide-binding domain of human CFTR with the regulatory insertion and extension excised.

Supplementary Table 1B. ***Closest structural homologs to ABC2 of E. coli EttA as identified by DALI.*** [a]

		ABCβ+Core 2					ABCα 2				
Protein	PDB [b]	Rank	Z-score	rmsd (Å)	% id	length	Rank	Z-score	rmsd (Å)	% id	length
EttA-ABC1		1	19.4	2.0	36	138	3	6.1	2.5	26	50
HI1470	2NQ2(C)	2	18.6	2.1	28	150	20	4.9	1.8	18	50
CFTR [b]	2PZE(B)	3	18.2	2.3	21	146	23	3.8	2.8	19	53
RLI	3BK7(A)	4	17.8	2.2	27	150	21	4.7	2.9	23	53
ArtP	2OLK(A)	5	17.8	2.8	24	154	12	5.3	1.9	17	52
FbpC	3FVG(A)	6	17.8	2.5	31	150	14	5.0	2.4	20	54
TM0544	1VPL(A)	7	17.4	2.8	30	153	21	4.8	2.1	18	50
EF3	2IX3(B)	10	17.1	2.8	32	148	2	6.2	2.3	23	53
BtuD	2QI9(B)	20	16.0	2.4	28	145	1	6.2	2.1	25	52

[a] The analyses were performed and the parameters are defined identically to Table S1A.

[b] This structure represents the first nucleotide-binding domain of human CFTR with the regulatory insertion and extension excised.

SUPPLEMENTARY NOTES

Possible models for the different activity of EttA in presence of ATP *vs.* ADP

Additional research will be needed to clarify many facets of EttA's mechanism and physiological function. Important mechanistic questions include how the two ATP-binding sites in EttA interact in the course of its functional reaction cycle and how ADP mediates EttA-dependent inhibition of synthesis of the first peptide bond in the nascent protein Our data show that WT-EttA has a qualitatively different effect on translation reactions conducted in the presence of ADP compared to either WT-EttA or EttA-EQ_2 in the presence of ATP (**Fig. 5** and **Fig. 4**). In the presence of ADP, WT-EttA inhibits synthesis of the first peptide bond by the 70S IC rather than promoting this reaction or trapping it following this reaction, as observed for WT-EttA and EttA-EQ_2, respectively, in the presence of ATP. Several models (see Supplementary Note) can be envisioned to explain this alternative activity in the presence of ADP compared to ATP. One possibility is that ADP interacts directly with the ribosome to alter its mode of interaction with EttA. This possibility is suggested by the small shift in the FRET efficiency distribution observed in the smFRET data recorded from the L1-L9 reporter pair on the 70S IC in the presence of ADP but not in the presence of ATP (**Supplementary Fig. 8b top *vs.* bottom**). An alternative possibility is that ADP binds directly to one or both of the ATPase active sites in EttA, resulting in an altered conformation that still binds to the 70S IC but stabilizes it in a conformation that inhibits formation of the first peptide bond rather than promoting it. In this case, there are several possible explanations for the different behavior of EttA upon directly binding ADP compared to the post-hydrolysis complex with ADP formed following the binding of ATP. One explanation is that peptide-bond synthesis on the ribosome while EttA is in the ATP-bound state pushes the ribosome into a conformation in which it is no longer sensitive to the ADP-bound conformation of EttA, which results in release of EttA from the ribosome following ATP hydrolysis. Another possibility is that transient electrostatic forces generated during the hydrolysis reaction induce the dissociation of EttA prior to adoption of its equilibrium ADP-bound conformation. A related mechanistic issue concerns whether there is functional asymmetry between the two ATPase active sites in EttA. Such asymmetry has been documented in ABCE1[12] and other members of the ABC superfamily having two ABC domains that differ in primary sequence. In this context, it is possible that one of the ATPase active sites in EttA plays a regulatory role and that binding of ADP to this site prevents adoption of the conformation promoting peptide-bond synthesis on the 70S IC even if ATP is bound to the other site. It also remains to be established whether ADP can be exchanged for ATP while EttA remains bound to the ribosomal E site or whether exchange can only occur after dissociation of EttA from the ribosome. Additional biochemical and biophysical studies will be needed to address these unresolved issues concerning the location of the ADP binding site influencing the activity of EttA and its mechanism of action.

Supplementary Methods

Protein expression and purification. All proteins expressed in a pBAD vector were grown in MG1655-*ettA::Tn5* strain in LB media (3 liter for all the constructs excepted EttA-EQ_2 which has very low expression and therefore was grown in 12 liter) to an OD_{600} of 0.6 and induced with 0.1 % of L-arabinose and grown for an extra three hours. Cells were centrifuged at 4,000rpm for 30 min (JS-4.2 rotor in Beckman J6-B), washed with Phosphate Buffered Saline (137 mM NaCl, 2.7 mM KCl, 10 mM, Na_2HPO_4, 2 mM KH_2PO_4) and then centrifuged for 10 min at 6,000 rpm in a GSA rotor (Sorvall).

To purify hexahistidine-tagged constructs (His_6-EttA-EQ_2, His_6-EttA-Δarm and His_6-EttA), pellets were weighed, stored at -80 ˚C, and resuspended in 5 ml per gram of cells of lysis buffer (150 mM NaCl, 10 mM imidazole, 2 mM 2-mercaptoethanol, 10% glycerol, 20 mM Tris-HCl, pH 7.5) supplemented with EDTA-free Complete Protease Inhibitor Cocktail Tablets (Roche). They were incubated 10 min on ice with 2 mg/ml of lysozyme (Sigma-Aldrich) and lysed using 3 passages through an Emulsiflex C3 (Avestin) at 16,000 psi. Lysates were centrifuged at 30,000 g for 30 min and loaded on Ni-NTA column (Qiagen). They were washed with 10 columns volume of buffer A (same as lysis buffer but without protease inhibitor), then with 10 columns volume of buffer B (same as A but with imidazole at 30 mM), and finally the protein was eluted with buffer C (same as A but with imidazole at 500 mM). The fractions containing the protein were pooled, concentrated and buffer exchanged (same as buffer A without imadazole) on a Amicon Ultra 30 kDa (Millipore). The concentrated proteins were then brought to 1M $(NH_4)_2SO_4$ prior to purification on a butyl-Sepharose FF column eluted with a 1000-0 mM gradient of $(NH_4)_2SO_4$ in the standard buffer (20 mM Tris-HCl pH 7.5, NaCl 150 mM, 10 mM imidazole, 2 mM 2-mercaptoethanol, 10% glycerol). The fraction containing EttA were pooled and buffer exchanged the same way as described previously.

For purification of untagged WT EttA, washed cell pellets were stored at –80 ˚C were thawed and resuspended in 5 ml per gram of cell with 10% glycerol, 5 mM DTT, Complete Protease Inhibitor Cocktail Tablets (Roche), 25 mM Tris-Cl, pH 8.0. Cells were lysed using 3 passages through an Emulsiflex C3 (Avestin) at 16,000 psi, and the extract was clarified by centrifugation 30 min at 30,000 g prior to purification on a DEAE-Sepharose FF column eluted with a 0-500 mM gradient of NaCl in the standard buffer (*i.e.*, the extraction buffer without protease inhibitor). EttA-containing fractions were then brought to 1M $(NH_4)_2SO_4$ prior to purification on a butyl-Sepharose FF column eluted with a 1,000-0 mM gradient of $(NH_4)_2SO_4$ in the standard buffer. EttA-containing fractions were pooled and purified on a Sephacryl S300HR gel filtration column (GE Healthcare) in the standard buffer plus 100 mM NaCl. The final protein pool was exchanged into the standard buffer. For the WT-EttA dimer monomer study the peaks corresponding to the monomer and the one corresponding for the dimer were concentrated separately. The dimer fraction was concentrated ~150 μM and was used for the static light-scattering experiment.

Selenomethionine labeled protein was expressed using the method of Le Master [13] in strain B834(λDE3). A 2 liter culture containing 30 μg/ml kanamycin sulfate and 50 mg/ml DL-selenomethionine was grown at 37°C to an OD_{600} of 0.6. At this point, 0.4 mM isopropyl 1-thio-

β-D-galactopyranoside was added and the cells were grown a further 2 hours with constant shaking. Cells were harvested by centrifugation and stored at -80˚C. All subsequent steps were carried out at 4˚C. For purification, harvested cells were mixed with 100ml buffer A (25mM Tris-HCl pH 8.0, 10% (w/v) glycerol, 2 mM phenylmethylsulfonyl fluoride, and 5 mM DTT) and homogenized using a French pressure cell at 20,000 psi. This cell lysate was clarified by centrifugation at 30,000 g for 30 min. Streptomycin sulfate was added to the resulting supernatant to a final concentration of 4% (w/v). The resulting mixture was incubated for 30 min followed by centrifugation at 30,000g for 30 min. After filtration through a 0.22 µm filter, the supernatant was loaded onto a 15 ml column of DEAE-Sepharose (GE Healthcare) equilibrated in Buffer A. Protein was eluted using a continuous gradient of 1M NaCl in Buffer A with EttA (as monitored by SDS-PAGE) eluting at ~250 mM NaCl. EttA containing fractions were then brought to 1M $(NH_4)_2SO_4$, filtered, and added onto a 50 ml column of Butyl-Sepharose (GE Healthcare) equilibrated in buffer A containing 1M $(NH_4)_2SO_4$. Proteins were eluted from the column using successively lower concentrations of $(NH_4)_2SO_4$. EttA containing fractions were then pooled, concentrated to 5 ml volume, and loaded on an S300HR size exclusion column (GE Healthcare) equilibrated in buffer A with 100 mM NaCl. EttA-containing fractions were pooled and desalted into buffer B (10 mM Tris-HCl pH 8.0, 10% glycerol, and 10 mM dithiothreitol), concentrated to ~240 µM, frozen in liquid nitrogen and stored at -80 ˚C.

Synthesis of mRNA for in vitro translation. A T7-luc mRNA was generated using the pBEST plasmid (Promega) as a template to amplify the gene of the luciferase (l*uc*). The PCR amplification was done first by using primer flanking the *luc* open reading frame; the forward primer contained the sequence compatible with the universal primer PURExpress (New England Biolab) kit which included a Ribosome Binding Site. Secondly, this PCR product was PCR amplified with the universal primer, which introduced the T7 promoter. This PCR product was gel purified using the gel extraction kit (Qiagen) and used as a template to generate a RNA with the T7 RiboMAX kit (Promega). The RNA was DNase treated and purified by Trizol extraction (invitrogen) and resuspended in the RNA buffer (Ambion). For the pT7gp32 mRNA, the RNA was produced using the same procedure, except without PCR amplification. The pT7gp32.1-224 plasmid [14] was linearized by restriction with BamHI and used as a template for the RiboMAX kit. The resulting RNA was purified as described above. The pT7gp32.1-20 mRNA used for the purified minimum translation assays was produced the same way as the pT7gp32.1-224, except that it used the pT7gp32.1-20 plasmid as a template. This plasmid has a stop codon after the residue 20 and the 4 first codons are AUG-UUU-AAA-GAA (Met-Phe-Lys-Glu).

In vitro translation using an E. coli S30 extract. T7-luc mRNA was used as a template for translation reactions conducted according to the manufacturer's recommendations using an extract purchased from Promega. In brief, the reaction contained 2.5 µl AA mix, 10 µl S30 premix and 7.5 µl S30 extract. Four µl of buffer or protein were assembled to test at the final indicated concentration on the graph. The reactions were started by adding 1 µl of T7-*luc* mRNA at 5 µg/µl and incubating at 37˚C for 2 hours. A 2 µl volume of each reaction was mixed with 50 µl of Luceferase Assay Reagent (Promega). Light emission was quantified with a luminometer for 10 seconds. Background was determined on a reaction without T7-*luc* mRNA and subtracted for the other measurements.

In vitro translation using purified components. The PURExpress system was purchased from New England Biolabs. Each reaction was carried out in a 5 µl total volume (2.5 µl of solution A, 1 µl of solution B, 0.5 µl of T7-luc mRNA at 2 µg/µl and 1 µl of buffer or protein to test at the final concentration indicated on the graph). Reactions were done in a 96 wells plate and in triplicate. After 2 hours of incubation at 37˚C, 1 µl of the reaction was mixed with 50 µl of Luciferase Assay Reagent (Promega). Light emission was quantified in a microplate reader in luminescence setup with 10 second read by well (Tecan Infinite 200 PRO). In vitro translation of pT7gp32.1-224 mRNA was performed with the PURExpress system (New England Biolabs) using [^{35}S]methionine In vitro Translation Grade (MPbio). The reaction contained 4 µl of solution A, 3 µl of solution B, and 1 µl of buffer or protein to test (EttA, EttA-EQ_2 and EttA EQ_2-*Δ*arm) at the final concentration of 5 µM and 1µl of [^{35}S]methionine (10 µCi). The protein was added before the mRNA (1st) or after the mRNA (2nd) or 15 min after addition of the mRNA (15'). The reactions were started by adding 2 µl of T7-*luc* mRNA at 0.5 µg/µl and incubating at 37˚C for 2 hours. The reactions were stopped by adding 20 µl of 2X Laemmli and heating for 2 min at 60˚C. Then 10 µl of each reaction were run on a 12.5% SDS-PAGE. The gel was stained and dried on Whathman as well as subjected to autoradiography, which is presented on this figure.

E site binding tRNA binding assays. For synthesis of deacylated [^{32}P]tRNA^{Phe} [15,16], 34 µM of tRNA^{Phe} (Sigma-Aldrich) was incubated with 50 mM of glycine pH 9, 10 mM $MgCl_2$, 360 Ci/mmol [α-^{32}P]ATP (Perkin Elmer), 0.05 mM sodium pyrophosphate and 0.03 mg/ml of nucleotidyl tranferase. The reaction was incubated for 5 min at 37˚C. Labeled tRNA was purified by phenol/chloroform extraction followed by ethanol precipitation, resuspension in milliQ water and filtration through a P6 column (Bio-Rad) pre-equilibrated with milliQ water in order to remove unincorporated radioactivity. Assessment of the stability of the deacylated tRNA bound in the E site as a function of $Mg(OAc)_2$ were done using an E site filter-binding assay based on the original assay of Grajevskaja *et al.*[17]. The 70S ribosomes used for the assay were prepared as for the minimal purified translation assay[14]. Reactions containing 70S ribosomes (0.2 µM) were incubated in presence of deacylated 0.4 µM [^{32}P]tRNA^{Phe} and increasing concentrations of $Mg(OAc)_2$ (3.5, 10, or 20 mM) for 1 min at 4 ˚C in a 20 µl reaction in 100 mM NH_4Cl, 20 mM Tris-HCl, pH 7.4. A 5 µl volume of each reaction was spotted on a nitrocellulose filter (25 mm, 0.45µm, nitrocellulose, disc filters, Millipore) installed on a Sampling Manifold (Millipore) under constant vacuum. After 3 washes with 2 ml of 20 mM $Mg(OAc)_2$, 100 mM NH_4Cl, 1mM EDTA, 20 mM Tris-HCl, pH7.4, the filters were transferred to scintillation fluid (Ultima Gold, PerkinElmer) and counted on a scintillation counter (Beckman LS6500). A 5 µl volume of each reaction was also counted. The radioactivity retained on the filter was divided by the total radioactivity and multiplied by the total concentration of radiolabeled tRNA to yield an estimate of the concentration of radiolabeled tRNA bound to ribosomes, which was divided by the total ribosome concentration for graphing as fractional occupancy of the E site.

ATPase Assays. ATP hydrolysis assays were performed in polymix buffer (5 mM Tris-OAc (pH 7.5), 95 mM KCl, 5 mM NH_4Cl, 5 mM $Mg(OAc)_2$, 0.5 mM $CaCl_2$, 2 mM 2-

mercaptoethanol, 5 mM putrescine, and 1 mM spermidine). To convert all ADP present in the reaction to ATP, solutions were pre-incubated at 37 ºC for 15 min with pyruvate kinase (PK) and phosphoenolpyruvate (PEP). Solution I consisted of [γ-^{32}P]ATP (100-200 dpm per pmol), 0.25 µg/µl PK, and 3 mM PEP in polymix buffer; solution II consisted of His_6-EttA, 0.25 µg/µl PK, and 3 mM PEP in polymix buffer. Reactions were carried out in 60 µl assays, with a final His_6-EttA and 70S concentration of 1 µM, respectively. ATP concentrations were varied as indicated (final concentrations). Background hydrolysis by ribosomal particles was also examined and subtracted if applicable; ribosome preparations typically did not have significant ATPase activity in these assays. Reactions were stopped with 50 µl of quenching solution (2 M perchloric acid with 3 mM KH_2PO_4). Then, 300 µl of 20 mM Na_2MoO_4 solution and 400 µl of isopropyl acetate were added and thoroughly mixed for 5 min. The organic phase was separated by centrifugation and the amount of liberated inorganic phosphate was quantified by scintillation counting (Perkin Elmer TriCarb 2800TR).

L1-L9 single molecule fluorescence energy transfer (smFRET$_{L1-L9}$) experiments. Populations of 70S ICs harboring a donor fluorophore (Cy3) on ribosomal protein L9 and an acceptor fluorophore (Cy5) on ribosomal protein L1 were imaged using total internal reflection fluorescence microscopy as previously described[18-20]. These experiments were performed in Tris-Polymix Buffer (50 mM Tris acetate (pH 7.0 at 25 °C), 100 mM KCl, 5 mM NH_4OAc, 0.5 mM $Ca(OAc)_2$, 0.1 mM EDTA, 5 mM putrescine dihydrochloride, and 1 mM spermidine free base) with 15 mM $Mg(OAc)_2$ and 10 mM 2-mercaptoethanol, supplemented with an oxygen-scavenging system (2.5mM 3,4-dihydroxybenzoic acid (PCA), 25nM protocatechuate 3,4-dioxygenase (PCD) and 1% (w/v) β-D-glucose). The small (30S) and large (50S) ribosomal subunits used for the formation of the 70S IC complex in smFRET$_{L1-L9}$ experiments were prepared as previously described[20]. The initiation factors, mRNA, and fMet-tRNA^{fMet} were prepared as previously described[14]. The 70S IC was formed in two steps. First, 30S subunits and L9(Cy3)-L1(Cy5)-labeled 50S subunits were incubated at 37 ^{o}C for 10 min in Initiation Polymix Buffer (Tris-Polymix Buffer in which the Mg(OAc) has been reduced to 5 mM and 2-mercaptoethanol has been reduced to 6 mM) at a final concentration of 1.2 µM, in the presence of 1.6 µM IF1, 1.2 µM IF2, 1.7 µM IF3, and 1 mM GTP. Second, 5'-biotinylated mRNA and fMet-tRNA^{fMet} were added to the above reaction to a finial concentration of 2.0 and 1.5 µM, respectively, prior to incubation for another 20 min at 37 ^{o}C. Once formed, the 70S IC was placed on ice for 15 min and purified using sucrose density gradient ultracentrifugation as previously described[14]. Independent trials recorded in the absence or presence of WT-EttA were recorded in a paired fashion. For these paired experiments, 100 pM 70S IC was pipetted into the flowcell in 15 mM $Mg(OAc)_2$ Tris-Polymix Buffer. After binding of the 5'-biotinylated mRNA 70S IC complex to the streptavidin-coated flowcell, the same buffer with Mg-ATP (2 mM) or Mg-ADP (2 mM) was added, and the smFRET data were recorded. Subsequently, 6 µM EttA in the same buffer with 2mM Mg-ATP or Mg-ADP was pipetted into the same flowcell, and the smFRET data were recorded. Independent experiments conducted in the in the absence or presence of 6 µM EttA-EQ_2 were performed in an unpaired fashion (*i.e.*, the data in the absence of EttA-EQ_2 were recorded from one flowcell, while the data in the presence of EttA-EQ_2 were recorded separately from a second flowcell).

SUPPLEMENTARY REFERENCES

1. Sievers, F. *et al*. Fast, scalable generation of high-quality protein multiple sequence alignments using Clustal Omega. *Mol Syst Biol* **7**, 539 (2011).
2. Waterhouse, A.M., Procter, J.B., Martin, D.M., Clamp, M. & Barton, G.J. Jalview Version 2--a multiple sequence alignment editor and analysis workbench. *Bioinformatics* **25**, 1189-91 (2009).
3. Diederichs, K. *et al*. Crystal structure of MalK, the ATPase subunit of the trehalose/maltose ABC transporter of the archaeon *Thermococcus litoralis*. *EMBO J* **19**, 5951-61 (2000).
4. Karpowich, N. *et al*. Crystal structures of the MJ1267 ATP binding cassette reveal an induced-fit effect at the ATPase active site of an ABC transporter. *Structure* **9**, 571-86 (2001).
5. Jones, P.M. & George, A.M. Subunit interactions in ABC transporters: towards a functional architecture. *FEMS Microbiol Lett* **179**, 187-202 (1999).
6. Hopfner, K.P. *et al*. Structural biology of Rad50 ATPase: ATP-driven conformational control in DNA double-strand break repair and the ABC-ATPase superfamily. *Cell* **101**, 789-800 (2000).
7. Smith, P.C. *et al.* ATP binding to the motor domain from an ABC transporter drives formation of a nucleotide sandwich dimer. *Mol Cell* **10**, 139-49 (2002).
8. Chen, B. *et al*. EttA binds at ribosomal E site and regulates translation by restricting ribosome dynamics.
9. Schneider, C.A., Rasband, W.S. & Eliceiri, K.W. NIH Image to ImageJ: 25 years of image analysis. *Nat Methods* **9**, 671-5 (2012).
10. Blanchard, S.C., Kim, H.D., Gonzalez, R.L., Jr., Puglisi, J.D. & Chu, S. tRNA dynamics on the ribosome during translation. *Proc Natl Acad Sci U S A* **101**, 12893-8 (2004).
11. Holm, L. & Rosenstrom, P. Dali server: conservation mapping in 3D. *Nucleic Acids Res* **38**, W545-9 (2010).
12. Barthelme, D. *et al*. Ribosome recycling depends on a mechanistic link between the FeS cluster domain and a conformational switch of the twin-ATPase ABCE1. *Proc Natl Acad Sci U S A* **108**, 3228-33 (2011).
13. Hendrickson, W.A., Horton, J.R. & LeMaster, D.M. Selenomethionyl proteins produced for analysis by multiwavelength anomalous diffraction (MAD): a vehicle for direct determination of three-dimensional structure. *EMBO J* **9**, 1665-72 (1990).
14. Fei, J. et al. A highly purified, fluorescently labeled in vitro translation system for single-molecule studies of protein synthesis. *Methods Enzymol* **472**, 221-59 (2010).
15. Ledoux, S. & Uhlenbeck, O.C. [3'-32P]-labeling tRNA with nucleotidyltransferase for assaying aminoacylation and peptide bond formation. *Methods* **44**, 74-80 (2008).
16. Wolfson, A.D. & Uhlenbeck, O.C. Modulation of tRNAAla identity by inorganic pyrophosphatase. *Proc Natl Acad Sci U S A* **99**, 5965-70 (2002).

17. Grajevskaja, R.A., Ivanov, Y.V. & Saminsky, E.M. 70-S ribosomes of Escherichia coli have an additional site for deacylated tRNA binding. *Eur J Biochem* **128**, 47-52 (1982).
18. Fei, J. et al. Allosteric collaboration between elongation factor G and the ribosomal L1 stalk directs tRNA movements during translation. *Proc Natl Acad Sci U S A* **106**, 15702-7 (2009).
19. Fei, J., Kosuri, P., MacDougall, D.D. & Gonzalez, R.L., Jr. Coupling of ribosomal L1 stalk and tRNA dynamics during translation elongation. *Mol Cell* **30**, 348-59 (2008).
20. Fei, J., Richard, A.C., Bronson, J.E. & Gonzalez, R.L., Jr. Transfer RNA-mediated regulation of ribosome dynamics during protein synthesis. *Nat Struct Mol Biol* **18**, 1043-51 (2011).